Source characteristics of ELF/VLF chorus

D. S. Lauben, U. S. Inan, and T. F. Bell
Space, Telecommunications and Radioscience Laboratory, Stanford University, Stanford, California, USA

D. A. Gurnett
Department of Physics and Astronomy, University of Iowa, Iowa City, Iowa, USA

Received 2 May 2000; revised 4 June 2001; accepted 23 July 2001; published 10 December 2002.

[1] Source characteristics of nonducted dawn-sector magnetospheric ELF/VLF chorus emissions are deduced from in situ chorus wave properties measured with the POLAR/PWI six-channel wideband wave receiver and applied as constraints to a simple chorus emission and propagation model. The model accounts for wave/particle resonance at the source and employs a multi-frequency ray tracing technique to estimate wave refraction and dispersion from source to receiver in order to accurately reproduce the observed frequency-time (*f-t*) spectral form and wave normal angle θ_p at the spacecraft, for some optimal combination of source L shell, magnetic latitude λ_s, and emission wave normal angle θ_s determined by iteration. The best-fit match for numerous chorus emissions observed over a dawn-sector orbit pass covering $3.5 < L < 6.5$ reveals that such chorus is generated consistently near the magnetic equator at latitudes $|\lambda_s| \leq 5°$, with chorus risers ($df/dt > 0$) produced on the opposite side of the equator with respect to the receiver, and chorus fallers ($df/dt < 0$) produced on the same side, in agreement with theory and simulation. The emission wave normal angle θ_s deduced at the source is found to be systematically related to the frequency band occupied by a given chorus element in order for waves to arrive at the spacecraft with the observed θ_p, in accord with Snell's law applied to the frequency-dependent topology of the respective whistler-mode refractive index surface. In particular, upper-band chorus waves ($f \geq 0.5\, f_{\mathrm{Heq}}$, where f_{Heq} is the equatorial gyrofrequency) are emitted with wave normal $\theta_s \simeq 0$, while lower-band chorus waves ($f \leq 0.5\, f_{\mathrm{Heq}}$) are emitted with $|\theta_s| \simeq \pm\theta_{\mathrm{G}}$, where θ_{G} is the so-called Gendrin angle giving minimum value of refractive index parallel to the static magnetic field. For both frequency bands, these respective θ_s values lead to wave propagation paths which remain naturally parallel to the static magnetic field in the source region over a latitude range of typically 3°–5°, providing ample opportunity for cumulative wave/particle interaction and thus rapid wave growth, notably in the absence of field-aligned cold plasma density enhancements (i.e., ducts). These results support a theory of nonducted chorus generation akin to that for ducted chorus, whereby each emission is seeded by embryonic noise at a resonance point located within a few degrees of the magnetic equator, wherafter rapid coherent wave growth at some starting frequency favored by the natural wave focusing effects set by prevailing magnetospheric conditions follows from interaction with subsequently phase-bunched counterstreaming electrons. For the common case of chorus risers, although the embryonic source point is located across the magnetic equator from the receiver as indicated for $df/dt > 0$, since the spatial wave growth profile increases in the direction towards the receiver and in fact reaches maximum intensity at or just beyond the magnetic equator, the waves appear to emanate from the equator itself. A symmetric ensemble of such chorus emissions thus produces waves which appear to propagate universally away from the magnetic equator, in accord with the observations of *LeDocq et al.* [1998]. *INDEX TERMS:* 2772 Magnetospheric Physics: Plasma waves and instabilities; 0689 Electromagnetics: Wave propagation (4275); 0654 Electromagnetics: Plasmas; 2753 Magnetospheric Physics: Numerical modeling; *KEYWORDS:* plasma wave, propagation, VLF chorus source, magnetosphere, wave/particle interactions

Citation: Lauben, D. S., U. S. Inan, T. F. Bell, and D. A. Gurnett, Source characteristics of ELF/VLF chorus, *J. Geophys. Res.*, *107*(A12), 1429, doi:10.1029/2000JA003019, 2002.

0148-0227/02/2000JA003019$09.00

1. Introduction

[2] Chorus, named for its characteristic sequence of continually repeating, usually rising ($df/dt > 0$), and often overlapping whistler mode ($f < f_H$, where f_H is the local electron gyrofrequency) coherent ELF/VLF tones (300 Hz – 12.5 kHz), ranks among the most intense of all naturally occurring ELF/VLF plasma wave emissions generated within the Earth's magnetosphere [*Gurnett and O'Brien*, 1964]. Chorus occurs regularly in association with disturbed magnetospheric conditions and is believed to be a driver of energetic electron precipitation on closed field lines in subauroral regions [*Tsurutani and Smith*, 1974; *Salvati et al.*, 2000], including microbursts, pulsating aurorae, and possibly morningside diffuse aurorae [*Inan et al.*, 1992 and references therein]. Chorus is observed both by spacecraft and at high-latitude ground stations.

[3] Chorus occurs typically in two distinct frequency bands, an upper-band just above ($\sim 0.5-0.6 f_{\mathrm{Heq}}$) and a lower-band somewhat below ($\sim 0.25-0.45 f_{\mathrm{Heq}}$) a frequency one-half the equatorial electron gyrofrequency (f_{Heq}) [*Tsurutani and Smith*, 1974; *Burtis and Helliwell*, 1969, 1976]. It has been suggested that this gap between frequency bands may be due to enhanced Landau damping at $0.5 f_{\mathrm{Heq}}$, which may quench and/or attenuate emissions which would otherwise span the gap to occupy both bands [*Tsurutani and Smith*, 1974]. Within either band, the frequency-time behavior of the individual discrete chorus emission regularly appear as either rising ($df/dt > 0$) and/or falling ($df/dt < 0$) spectral forms and sometimes manifest upward and/or downward hook-shaped features (df/dt inflections).

[4] Chorus appears to be generated during episodes of enhanced anisotropy in the energetic (10–100 keV) electron distribution within spatial regions surrounding a local minimum in the static magnetic field intensity [*Burton and Holzer*, 1974; *Burton*, 1976; *Tsurutani and Smith*, 1977; *Isenberg et al.*, 1982; *Sazhin and Hayakawa*, 1992; *Trakhtengerts*, 1995, 1999 and references therein]. Apparently, chorus can be generated in either ducted and nonducted modes, depending on the presence or absence of field-aligned gradients in the cold plasma density beyond the plasmapause [*Burton and Holzer*, 1974].

[5] Numerous theoretical treatments of chorus have been offered, and the interested reader is referred to the reviews by *Omura et al.* [1991], *Sazhin and Hayakawa* [1992], and references therein. In particular, *Trakhtengerts* [1999] has presented a fresh treatment of chorus in terms of the backward-wave oscillator mechanism first applied by *Helliwell* [1967] to the closely related case of artificially triggered VLF emissions. Note that for tractability, theoretical treatments are limited primarily to the case of ducted chorus, for which the wave normal angle is taken as everywhere parallel to the static magnetic field.

[6] Significant advances in the numerical simulations of chorus emissions have also been published. *Nunn et al.* [1997] have presented a Vlasov code able to reproduce repeating individual discrete rising chorus emissions as observed on GEOTAIL, while *Smith and Nunn* [1998] used the same approach to reproduce VLF risers, fallers, and hooks emissions observed at ground stations in the Antarctic. As with the theoretical work, these simulations are also generally restricted to the case of ducted chorus, owing to the great complexity and increased computation load required to handle the additional degrees of freedom associated with nonducted wave/particle resonance and wave propagation modes.

[7] Nonetheless, chorus is generated in the nonducted mode apparently quite regularly, as indicated by in situ measurements of the wave normal angles close to or in the actual emission region. *Burton and Holzer* [1974] gave the first measurements of chorus source wave normal angles θ_s using OGO-5 data and found in particular that nightside chorus manifest a wave normal cone with 20° half-angle about the local static magnetic field for sources determined to be within 2° of the magnetic equator. *Goldstein and Tsurutani* [1984] presented further OGO-5 measurements of θ_s for generally lower-band chorus at locations within 5° of the magnetic equator, and thus close to the presumed generation region. They reported an average value of $\theta_s \simeq 12°$, with some angles near the so-called Gendrin angle [*Stix*, 1962], although for reduced wave power. *Hayakawa et al.* [1984] provided similar measurements of wave normal angles at $L \simeq 6.6$ near-equatorial regions using GEOS-2 data and showed angles for lower-band chorus in the range $\theta_s \simeq 5°-20°$ for slower df/dt, with $\theta_s \simeq 30°-45°$ for faster df/dt slopes, while those for upper-band chorus were found to be close to the resonance cone, with some variation associated with differing df/dt slope.

[8] Chorus waves can and do propagate many hundreds of kilometers away from the generation region, in both the ducted and nonducted mode, provided they remain sufficiently electromagnetic in nature [*Burtis and Helliwell*, 1969; *LeDocq et al.*, 1998]. A few researchers have considered the propagation of such whistler-mode waves away from the emission source. *Burtis and Helliwell* [1969] presented early ray tracings of chorus waves from the point of observation back to the presumed source region at the equator assuming nonducted wave propagation.

[9] *Lefeuvre and Helliwell* [1985] used two-dimensional ray tracing analysis applied to GEOS-1 chorus (and hiss) to determine the variation in wave normal angle along the ray path in the source magnetic meridian from a presumed equatorial generation region to off-equatorial observation points. Their results included the hypothetical case where under certain conditions, bifurcating ray paths associated with distinct wave normal angles diverging from a given source point may later reconverge at a given distant observation point, leading to clustering of observed wave normal angles about more than one value.

[10] *Cairo and Lefeuvre* [1986] applied *three*-dimensional ray tracing to the related case of VLF Hiss, showing that whistler-mode wave energy may deviate by up to $\sim 10°$ in longitude away from that of the source. *Muto et al.* [1987] used similar three-dimensional ray tracing analysis to interpret GEOS–1 observations of upper-band VLF emissions (including chorus) for which the wave normal angles were close to the resonance cone and found results consistent with longitudinally distributed sources falling into two L-shell regions, inside and beyond $L = 6.6$. *Hayakawa et al.* [1990] presented further measurements of wave normal angles of lower-band chorus on GEOS-1, suggesting that further ray tracing is in general greatly needed to unravel the propagation effects and determine the source region.

[11] In principle, chorus waves contain information regarding the emission mechanism by which they were generated, and a few researchers have attempted to deduce characteristics of the underlying wave/particle generation mechanism based on features and properties of chorus waves received at remote locations. In particular, the wave normal angle at the source is of principle interest since it has fundamental bearing on the underlying wave/particle interaction process leading to the excitation of chorus waves. Such efforts necessarily require a comprehensive end-to-end model for emission generation, propagation, and measurement chain. In this regard, *Skoug et al.* [1996] have shown consistency between a cyclotron resonance model for VLF chorus emissions and certain chorus risers observed by a sounding rocket launched from Poker Flat, Alaska, by virtue of frequency-time match, appealing to warm-plasma wave modes in order to extend the resonance condition to reach the observed upper frequency limit. *Lauben et al.* [1998] combined six-channel POLAR PWI data with two-dimensional ray tracing in demonstrating the relationship between chorus intensity and solar wind dynamic pressure for chorus emission sources, found to be located within a few degrees of the magnetic equator with wave normal angles significantly different from zero, and deduced that the energies of the responsible electrons were likely in the range 14–30 keV. Most recently, *LeDocq et al.* [1998] used six-component Poynting vector measurements from Plasma-wave Instrument (PWI) to show that the direction of chorus wave power flow is universally away from the magnetic equator.

[12] A full explanation of chorus must elucidate the relationship between the specific energetic particle distributions responsible for the emissions and the detailed properties of the waves measured at remote locations, taking into account path-dependent propagation effects. Towards this end, in this paper, further use is made of six-channel vector waveform data from PWI to measure the precise frequency-time form and wave normal angles of selected discrete chorus emissions over a representative orbit pass. Consideration is given to chorus observed in the postmidnight to prenoon sector for $L < 6.5$, where the static magnetic field lines are generally the least disturbed, thus simplifying the models and interpretation [*Goldstein and Tsurutani*, 1984]. These measurements are applied as constraints to a simple chorus emission model which accounts for the wave/particle resonance condition at the source and for source to receiver ray path refraction and dispersion, in order to reproduce the frequency-time (*f-t*) spectral form and wave normal angle θ_P measured at the spacecraft, for some optimal combination of source L shell, magnetic latitude λ_s, and emission wave normal angle θ_s. The results developed herein indicate that the most general chorus treatment must include the case for which wave normals at the source may be significantly nonzero.

2. Chorus Measurements

[13] Chorus observations are made with the Plasma Wave Instrument (PWI) aboard the POLAR spacecraft. POLAR follows a $\sim 90^\circ$ inclination, $\sim 2 \times 9$ R_E, ~ 18 hour period, North Pole apogee orbit [*Harten and Clark*, 1995], and samples field lines typically $L < 8$ for magnetic latitudes $|\lambda| < 30^\circ$, crossing the magnetic equatorial plane for L in the range $2.5 < L < 4.5$, usually just inside the plasmasphere. The PWI sensors include one spin-axis aligned electric dipole (14 m), two orthogonal spinning (6 s period) electric dipoles (100 m, 130 m), and three orthogonal magnetic search-coils (70 nT^2 Hz^{-1} sensitivity). The PWI electronics include a Swept Frequency Receiver (SFR) which provides continuous single-component E, B data (covering 26 Hz - 810 MHz at better than 1 min resolution), and a High-Frequency Waveform Receiver (HFWR) which provides coincidently sampled six-component wideband (0–26 kHz) **E**, **B** vector wave field snapshots of duration ~ 0.45 s at spacing 9.2 s [*Gurnett et al.*, 1995].

[14] Figure 1 shows wave activity observed by the SFR near the dawn meridian for a 90 min interval covering the orbit trajectory shown in Figure 2. Chorus wave energy is evident in Figure 1 starting at ~ 1 kHz at 1940 UT and roughly follows the $0.35 f_{\mathrm{Heq}}$ and $0.5 f_{\mathrm{Heq}}$ reference lines throughout the interval. The shaded region of Figure 2 represents the plasmaspheric electron density (assumed to be in diffusive equilibrium) deduced from the f_{UHR} line evident in Figure 1 [*Carpenter et al.*, 1981]. For this epoch the density profile beyond the plasmapause is quite smooth; specifically, no significant field-aligned density gradients (i.e., ducts) are manifest. Note that POLAR enters the plasmasphere shortly after 2020 UT and emerges shortly after 2100 UT as indicated in Figure 1 by the rise and fall in f_{UHR} and in Figure 2 by the sharp increase in derived cold plasma density (>50/cc). Chorus wave energy is essentially absent inside the plasmasphere; any trace levels are *likely* due to leakage from regular emissions occurring beyond the plasmapause.

[15] Figure 3 shows a representative six-channel, 0.45 s duration wideband snapshot spectrogram revealing two discrete upper-band chorus emissions captured just beyond the plasmapause, very close to the magnetic equator. The left column shows the data in spinning spacecraft coordinates $(u, v, z)_{sc}$ for each of the three electric antennas and three magnetic search coils. The right column shows these same data in despun, local-field-aligned coordinates $(x, y, z)_{fa}$, where the despun and transformed z direction is taken parallel to the local static magnetic field $\mathbf{B_o}$, x lies in the magnetic meridian, and y completes the right-hand coordinate system. All six components show reasonably good signal to noise ratio (the spinning E_z and field-aligned E_y panels have elevated noise floors due to the order of magnitude shorter dipole), and the significant magnetic wave energy indicates that these emissions are electromagnetic as opposed to electrostatic. Although many chorus emissions are considerably more intense than these, the clean isolation from neighboring chorus emissions and extremely narrowband character of this pair render them especially suitable for wave normal and phase coherency analysis.

[16] Figure 4a highlights the transverse (to $\mathbf{B_o}$) wave magnetic field component B_y of the stronger emission at higher resolution $\Delta f = 35$ Hz, $\Delta t = 10$ ms. Note that the B_y component best represents the chorus emission since it is typically the least affected by changes in wave normal angle along the propagation path. Five markers ranging from $f_1 \simeq 9.2$ kHz, $t_1 \simeq 0.04$ s to $f_2 \simeq 10$ kHz, $t_2 \simeq 0.42$ s identify five typical *f-t* points used to represent this chorus element in the multi-frequency ray tracing analysis of section 3.

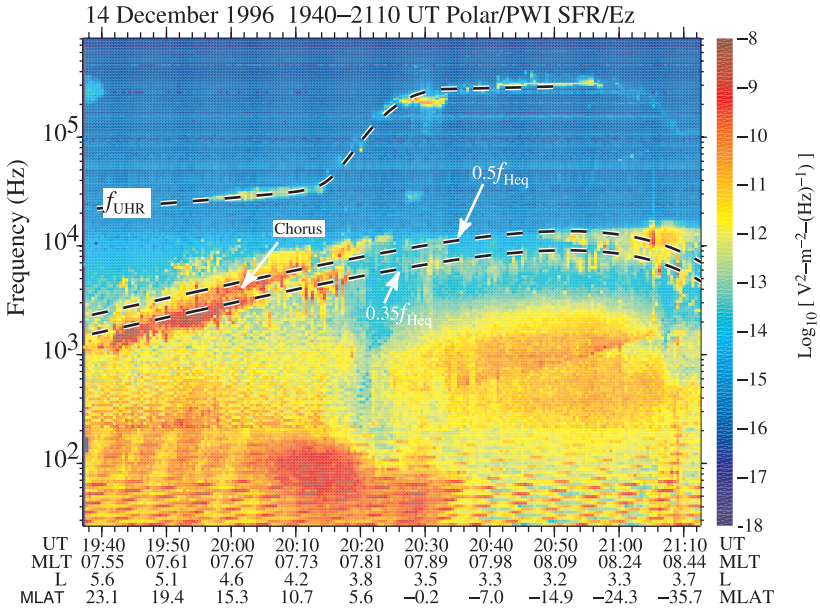

Figure 1. POLAR/PWI SFR spectrogram showing chorus in two bands (middle-region) and f_{UHR} resonance line (upper-region), from which cold plasma density is derived.

[17] Figure 4b shows the intensity of the selected chorus emission over time as determined by a digital frequency tracking filter of bandwidth $\Delta f = 35$ Hz centered about the spectral form. The intensity of this B_y component ranges ~0.5 pT to 1.2 pT, again rather low for chorus, but nonetheless providing ample noise margin for further signal processing. In fact, such a low intensity measured so close to the source (as will be shown in section 3) may actually have great significance regarding the trapping threshold for non-linear wave/particle resonance and sustained wave power saturation levels [*Bell*, 1986; *Helliwell et al.*, 1980].

[18] Next, a Fourier implementation of Means' method [*Means*, 1972; *Hayakawa et al.*, 1990; *Lauben et al.*, 1999] is applied to the three-component vector wave magnetic field **B** in conjunction with the sign of **E** × **H** to determine unambiguously the spectrally-resolved **k** vector (i.e., normal to planes of constant wave phase) for each Δf-Δt cell along the selected chorus emission in Figure 4a. The angle which

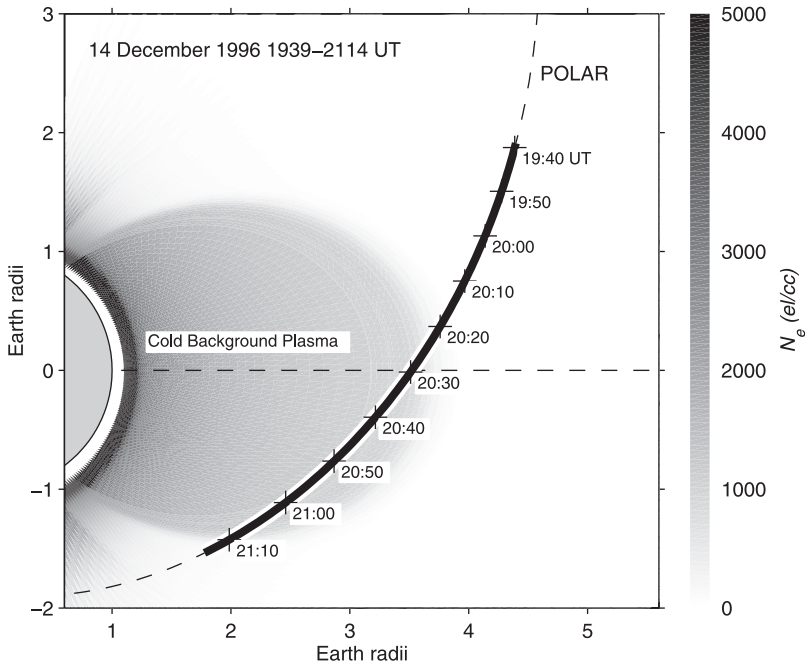

Figure 2. POLAR orbital trajectory on 14 December 1996. The background cold plasma density is derived from measurements of the upper hybrid frequency f_{UHR} and is indicated by the grayscale with density given by scale bar.

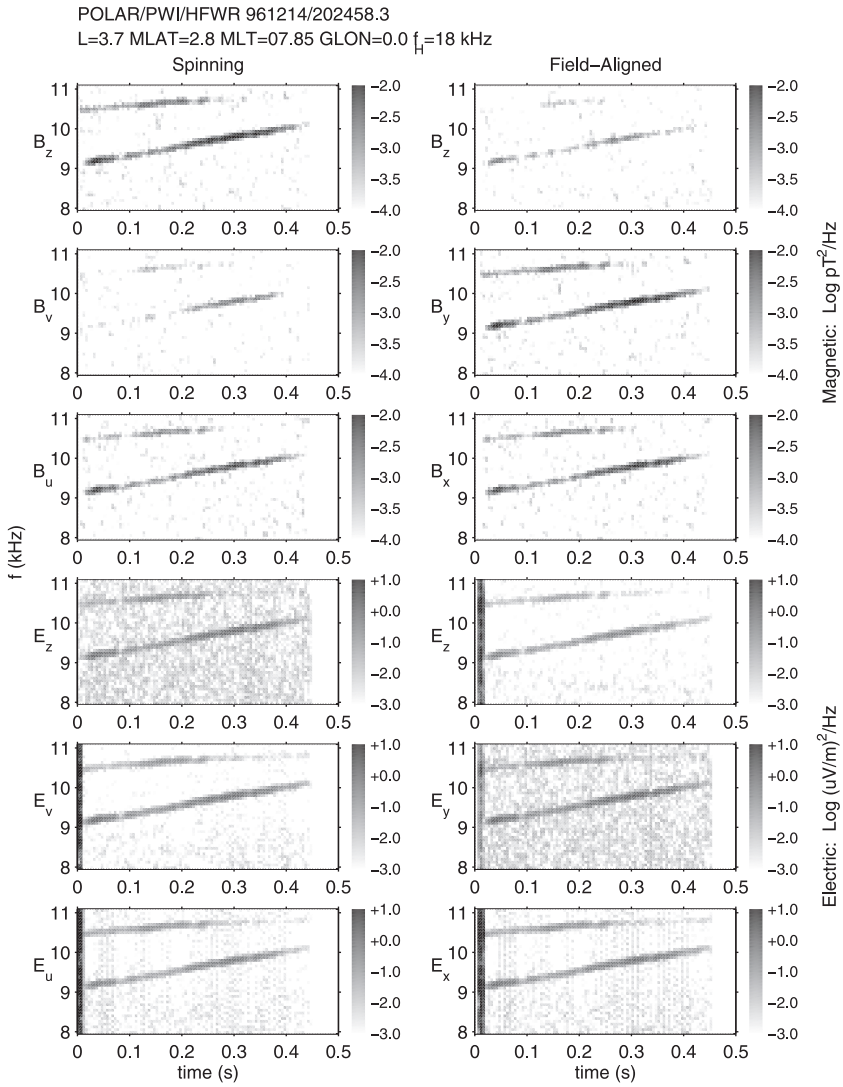

Figure 3. POLAR/PWI six-channel wideband snapshot data showing the three electric and three magnetic field components in both spinning (raw data) and field-aligned coordinates. Two discrete chorus emissions are apparent, both of which are above the equatorial half gyrofrequency on the field line of observation.

k then makes with the local magnetic field $\mathbf{B_o}$ is precisely the wave normal angle θ_p which is applied as a boundary constraint to the chorus model of section 3 (throughout this paper, the subscript p denotes a value measured at the point of observation, while s denotes a value deduced at the source location).

[19] While other wave normal estimation techniques are available, the use of Means' method is particularly well-suited to this study since (1) the search coils are well-matched in calibration, (2) the wave energy is believed to be comprised of one dominant electromagnetic mode, and (3) no knowledge of the surrounding plasma medium is required. Note that the particular algorithms employed herein have been verified against Omega transmitter signals and natural VLF whistlers [*Lauben et al.*, 1999].

[20] Figure 4c shows the extracted wave-normal angle θ_p over the selected chorus emission. The θ_p at each time step (open circles) is the average θ_p for the group of Δf-Δt cells above and below the emission center frequency which manifest wave energy within 3 dB of the strongest Δf-Δt cell at a given point in time. Here the θ_p values are scattered over the range $\sim$5° to $\sim$50° and have mean value of $\sim$25°, indicated by the solid line. The dashed lines above and below the mean show the $\pm 1\sigma$ data scatter. As a check, the use of alternate dynamic spectrum resolution Δf-Δt parameters was found to produce a slightly different scatter pattern, but to leave the mean and standard deviation essentially unchanged. In addition, a $\mathbf{B} \times \dot{\mathbf{B}}$ calculation applied in the time-domain to an appropriately band-limited version of the selected chorus signal was seen to yield similar values for these parameters, with a more or less Guassian distribution about the mean value.

[21] Considering that waves which are highly coherent can interact with charged particles more strongly than waves which are predominantly stochastic, it is of interest to examine the phase coherency of the chorus emission to gain better insight into the underlying wave/particle interaction mechanism. To be most meaningful, such phase

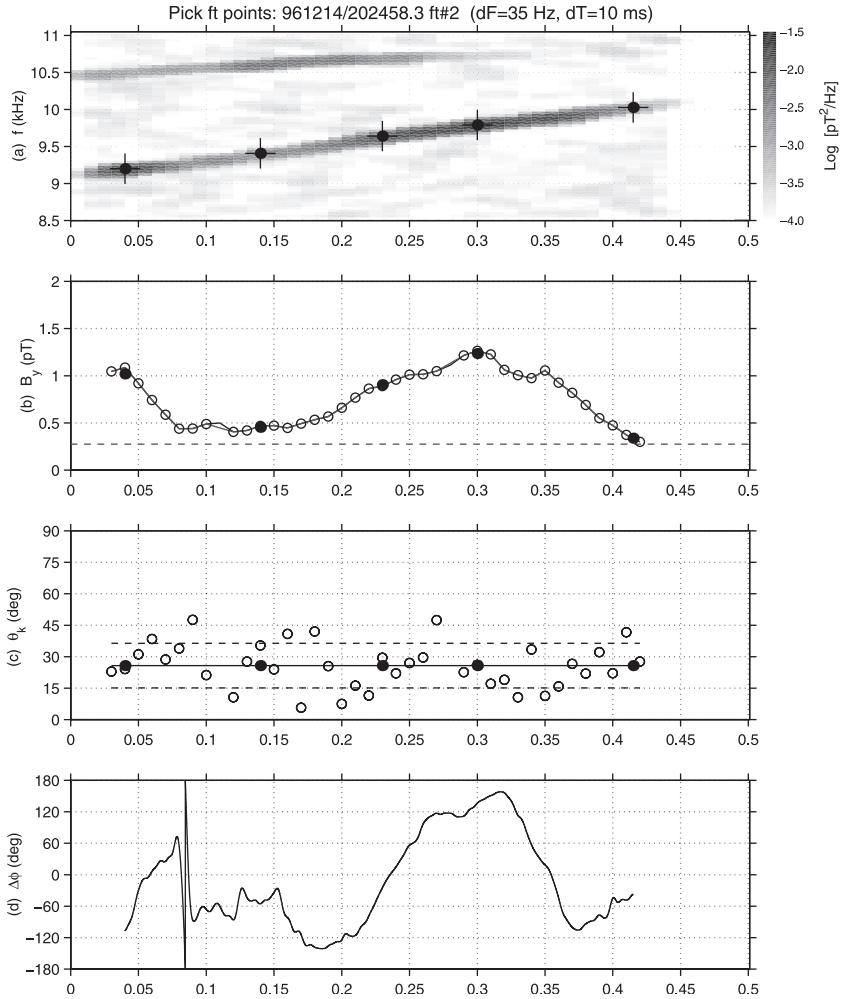

Figure 4. The **k**-vector directions extracted from data shown in Figure 3 using Means [1972] method. Isolated upper-band chorus riser. (a) Dynamic Spectrogram of B_y component. (b) Measured B_y intensity along emission *f-t* trace. (c) Measured wave normal angle θ_k^m. (d) Coherent phase with respect to an ideal reference signal derived from Figures 4a and 4b.

measurement should null out the first-order phase advance associated with the basic *f-t* ramp behavior of the chorus emission. This can be done as follows: First, an analytic time-domain frequency ramp signal is defined as

$$X_a(t) = \exp\left\{ j\,2\pi \int f(\tau) d\tau,\right.$$

where $f(\tau)$ represents a low-order polynomial fit to the spectral form of Figure 4a. The instantaneous phase of the fitted frequency ramp $X_a(t)$ thus provides a meaningful reference to which the phase of the actual chorus signal may be compared. Then the time-dependent complex scalar $b_y(t)$ is found which relates the measured chorus signal $B_y(t)$ to $X_a(t)$ as

$$B_y(t) = [b_y(t)][X_a(t)],$$

whence $\Delta\phi(t) = \arg\, b_y(t)$ gives the phase deviation between $B_y(t)$ and $X_a(t)$.

[22] Figure 4d plots $\Delta\phi(t)$ for this example. Here $\Delta\phi(t)$ is seen to vary in a more or less smooth manner over the life of the chorus emission, remaining within $\sim\pi$ radians of the phase of $X_a(t)$. In other words, so long as the signal remains sufficiently strong, the phase tracks that of an idealized chorus element within one wave cycle. This same smooth $\Delta\phi(t)$ behavior is replicated for all six field components.

[23] The smoothness of $\Delta\phi(t)$ relates directly to the coherence and phase stability of the underlying natural emission process, and in particular implies that any motion of the emission source must be itself smooth and well behaved. Application of this analysis technique to additional chorus emissions consistently reveals similarly smooth phase continuity, which suggests that as a rule, the basic nature of the chorus emission process is fundamentally highly coherent. Such coherency in turn implies that wave growth from embryonic to maximum levels may be possible within a few wave cycles over relatively small spatial scales.

3. Chorus Source Determination

[24] The procedure used to identify the location and characteristics of the source associated with a particular chorus emission involves first tracing rays from the space-

craft back to the magnetic equator based on the observed θ_p to obtain an initial estimate of the source field line, and then re-tracing rays forward from source to receiver while applying certain additional constraints to ensure a viable wave/particle resonance condition at the source and a good match to θ_p and the frequency-time spectral form at the spacecraft. The constraints applied at the source describe a simple chorus emission model having as free parameters the source field line L_s, magnetic latitude λ_s, and emission wave normal angle θ_s, and accounts for any intrinsic *df/dt* produced at a quasi-stationary off-equatorial resonance point (as discussed below). The ray tracing technique uses a multi-frequency approach to account for the additional group delay and frequency-time dispersion from source to receiver. An error term is defined to penalize trial emissions which arrive at the spacecraft with the wrong wave normal angles or incorrect spectral form or which miss the spacecraft altogether. The free parameters are seeded with those values found in the first step and then iterated to find the optimum combination giving minimum error. The final L_s, λ_s, and θ_s are then taken as those which best represent the true source. What follows is a detailed description and rationale of the essential features of the model.

3.1. Initial Source Location

[25] The first step is to identify the approximate source field line L_s, latitude λ_s, and emission wave normal angle θ_s, used to seed the emission and forward ray tracing model by tracing rays from the spacecraft back to the magnetic equator. Although finding L_s and θ_s for an assumed equatorial source given the observed θ_p is essentially a deterministic calculation, the uncertainty in θ_p leads directly to uncertainty in L_s and θ_p which thus warrants iteration over the search space so defined. Nor is it a forgone conclusion that the reverse rays paths should be terminated exactly at the magnetic equator $\lambda_s \simeq 0$, since the point of minimum inhomogeneity in the static magnetic field line may be displaced from the magnetic equator depending on L shell, magnetic local time, magnetic storm conditions, and other factors [*Tsurutani and Smith*, 1977].

[26] However, six-channel $\mathbf{E} \times \mathbf{H}$ Poynting vector measurements from PWI [*LeDocq et al.*, 1998] over many POLAR orbit passes show that for conditions consistent with the present case, the absolute direction of chorus wave power flow is universally away from the magnetic equator. Specifically, the direction of wave power flow is seen to change abruptly from northward to southward on opposite sides of the magnetic equator as the spacecraft crosses the magnetic equatorial plane. Conversely, chorus wave energy does not appear to flow toward the magnetic equator from higher absolute latitudes, or if it does, it is masked by the much strong chorus waves propagating away from the equator from an approximately mirror-image source. These results argue strongly that the source for these chorus emissions is located very close to, if not at, the magnetic equator itself, so it indeed seems appropriate to trace rays back to the equator, and in fact slightly beyond, for reasons which are explained below.

[27] For the chorus emissions considered herein, the **k** vector (see section 2) is found to lie within ±30° of the magnetic meridian; in such case the longitudinal deviation of the ray paths is minimal, so that two-dimensional ray tracing in the magnetic meridian is sufficient to resolve the ray paths with negligible error [c.f., *Lefeuvre and Helliwell*, 1985]. The particular ray tracing code employed [*Inan and Bell*, 1977] assumes a dipole model for the Earth's magnetic field and derives the cold plasma density profile from the upper-hybrid resonance profile manifest in the SFR spectrogram (Figure 1) [*Carpenter et al.*, 1981]. In tracing these ray paths, the scatter in the measured θ_p evident in Figure 4c translates directly into uncertainty as to the precise equatorial source L shell predicted by the ray tracing procedure. Accordingly, three sets of five ray paths are considered (one ray path per frequency point indicated by the filled circles in Figure 4a), the first set associated with the nominal average wave normal value denoted $\bar{\theta}_p$ and two others associated with $\bar{\theta}_p \pm \sigma_\theta$. Altogether, 15 ray paths are traced from the spacecraft back towards the magnetic equator.

[28] Finally, as there is indication from simulations [*Nunn and Smith*, 1996], [*Nunn et al.*, 1997] that the latitude boundaries of the full interaction region may be up to several degrees from the magnetic equator, in particular for the low-amplitude, so-called upwave point [*Nunn et al.*, 1997], c.f. *Helliwell* [1967], the rays are not yet terminated at any particular southern latitude, pending application of the chorus emission model.

3.2. Chorus Emission Model

[29] The wealth of literature regarding wave/particle interaction mechanisms from *Dowden* [1962] and *Brice* [1963] on up through *Trakhtengerts* [1999] contains a number of demonstrated and proposed features which would seem to apply, either directly or by extension, to the present case of nonducted chorus generation. Summarized below are features common to the various prevailing theories of chorus generation. While not all features may necessarily apply to the present case, the chorus model developed here is sufficiently general to allow complete for such consistency where required.

[30] First, it is commonly believed that magnetospheric emissions such as chorus are generated by a Doppler-shifted gyroresonance interaction between whistler-mode plasma waves and counter-streaming energetic electrons for which the instantaneous velocity $v_\parallel$ of the resonant electrons is related to the instantaneous properties of the waves by [*Vomvoridis et al.*, 1982; *Trakhtengerts*, 1995],

$$v_\parallel = \frac{\omega_H - \omega}{k_\parallel}, \tag{1}$$

where ω is the wave frequency, $k_\parallel$ is the wave number parallel to the static magnetic field, and ω_h is the local electron gyrofrequency. Note that a quick calculation using (1) for the example case ($f_{\mathrm{Heq}} \simeq 17.2$ kHz, $f \simeq 10$ kHz, and wave number $k \simeq 0.004$ from the ray tracer output) gives $v_\parallel = 11 \times 10^6$ m/s. Meanwhile the distance along the field line for a reasonable wave/particle interaction length of ~3° is $\Delta z \simeq 1.2 \times 10^6$ m, which means that a given particle bunch moving at this velocity passes through the interaction region in ~1/10 s, or roughly 1/5 the duration of the chorus emission. Applying a standard argument, if the wave emission point were to follow a single particle bunch moving down the field line at $v_\parallel$, then by the end of the ~1/2 s emission it would be at $\lambda \simeq 15°$, well in violation of the observations of *LeDocq et al.* [1998]. Consequently, in

order for the source region to remain in the vicinity of the magnetic equator for the duration of the emission, a continuous stream of fresh incoming particles must continually replenish and sustain the interaction during that time.

[31] Second, the highly coherent nature of the emitted waves as shown in Figure 4d, in combination with the transverse phase bunching of resonant particles known to occur for interactions with waves exhibiting such high coherency, suggests that the wave energy radiated by each loop of the resulting helical current structure formed by the particles likely adds coherently along the direction of wave propagation [*Brice*, 1963; *Dysthe*, 1973; *Helliwell and Crystal*, 1973]. While such coherent addition along the direction of wave propagation is not required, if it does take place, the source can be treated as more spatially compact and efficient. Note that a compact source is already implied by *LeDocq et al.* [1998], and that very early, *Nunn* [1971] predicted that the resonant particle current should be produced by a small number of particles closely confined in velocity space, pointing out that the particle inertia will ultimately ensure narrow band emissions.

[32] Third, factors must be present to give rise to nonzero *df/dt* slope from an otherwise quasistationary source, as identified above. A factor giving nonzero *df/dt* at a stationary point in an inhomogeneous magnetic field was described by *Helliwell* [1967], who noted that as waves emitted by a given ensemble of resonant particles at a given interaction point subsequently propagate upstream toward fresh incoming electrons, the change in resonance condition at upstream locations necessarily selects a new, ever-changing cut in particle phase space, so that as each new particle ensemble arrives at the original downstream interaction point, new waves are radiated at a correspondingly different frequency.

[33] The requirement for a continuous supply of fresh incoming resonant particles moving through the interaction region in combination with the continual frequency change over time has important implications regarding the latitude λ of the interaction region. *Helliwell* [1967] gives a formula to predict *df/dt* as a function of the latitude of a so-called "phase equator" at which the changing emission frequency balances the static magnetic field inhomogeneity. This formula has been validated independently by several researchers, including *Dowden* [1971], who accurately deduced the prevailing cold plasma electron density profile by matching the observed *f-t* spectral forms of triggered emissions, by *Skoug et al.* [1996], who matched chorus risers observed on a sounding rocket, and more recently by *Lauben et al.* [1998], who matched chorus risers observed by POLAR near the dawn meridian during a substorm onset episode, using an early implementation of the model developed herein.

[34] In addition, *Dysthe* [1971] discussed mathematical conditions for which a linear frequency change with time can occur, essentially defining a phase equator akin to *Helliwell* [1967]. At the same time, *Nunn* [1971] pointed out that the reactive component of the resonant particle current is independently able to cause a steady change in the wave frequency over time by imposing a wavelength shift over distance. Since then, several comprehensive theoretical treatments which incorporate known *df/dt* factors have been published, including *Nunn* [1974, 1990], *Nunn and Smith* [1996], *Nunn et al.* [1997], *Vomvoridis et al.* [1982], *Omura and Matsumoto* [1982], *Molvig et al.* [1988], and *Trakhtengerts* 1995, 1999]. For a good discussion of these various *df/dt* terms and their relative importance, the reader is referred to *Omura et al.* [1991], *Nunn and Smith* [1996]; *Nunn et al.* [1997], and *Smith and Nunn* [1998].

[35] Most notably for the present model, *Nunn et al.* [1997] defines a wave amplitude factor R and net inhomogeneity factor S and finds that during simulation, the point defined by $S = 0$, equivalent to the phase equator of *Helliwell* [1967], turns out to be a limiting latitude furthest from the equator where resonance first begins, whereas (for the case of equatorward propagating waves giving chorus risers) the latitude of maximum spatial wave growth occurs somewhat closer to the equator at points defined by $0.5 \leq |S/R| \leq 0.8$. Both *Nunn and Smith* [1996] and *Nunn et al.* [1997] note general agreement between their simulation results and the prediction of *Helliwell* [1967] that fallers are generated on the same side of the magnetic equator with respect to the point of observation, while risers are generated on the opposite side. Furthermore, *Nunn and Smith* [1996] explicitly remarks that the low wave amplitude point of the simulated chorus interaction region was indeed found to be near the $S = 0$ *Helliwell* [1967] phase equator.

[36] Although the calculation of explicit resonant particle current in the manner of *Nunn and Smith* [1996] and *Nunn et al.* [1997] is beyond the scope of this present study, the comments therein regarding the distinction between the $S = 0$ and $0.5 \leq |S/R| \leq 0.8$ points can be brought into the present context by simply considering that in the moments before a significant resonant current structure forms, the only non-zero *df/dt* factor at play for any potential resonance point is precisely the $S = 0$ phase equator term associated with the local inhomogeneity. Thus the phase equator or $S = 0$ latitude defined by *Helliwell* [1967], hereafter denoted λ_{S0}, retains significance as the point at which the embryonic emission likely first takes hold, and thus has great utility as an easily calculable bound on the wave/particle interaction point which for risers is the most distant from the magnetic equator, and for fallers, is the point closest to the equator.

[37] For the present effort, a formula is required which estimates *df/dt* at a given limiting interaction latitude λ_{S0} for nonzero chorus emission wave normal angles $|\theta_s| \geq 0$. Accordingly, equation (15) of *Helliwell* [1967] is generalized to become (see appendix):

$$\frac{df}{dt} = \frac{v_g}{1 + v_g/v_\parallel}\left[\frac{3\Lambda\cos\theta_s - \Lambda^2(\cos\theta_s + 2)}{(1+\Lambda)\cos\theta_s - 2\Lambda^2}\right]\frac{df_H}{dS}, \qquad (2)$$

where $\Lambda = f/f_H$, v_g is the wave group velocity, $v_\parallel$ is the particle parallel velocity, and df_H/dS is the local rate of change in gyrofrequency with linear distance along the field line. The relation to λ_{S0} is implicit through this last term. To summarize the forgoing discussion, when (2) is used to identify a particular λ_{S0} for which the calculated *df/dt* matches some observation, the value of latitude so obtained identifies the point of likely embryonic resonance, which for chorus risers slightly overestimates the latitude of maximum spatial wave growth, and for chorus fallers slightly underestimates this point.

[38] Note that since λ_{S0} is identified as the low amplitude embryonic point of the effective end-fire antenna array as described by *Nunn and Smith* [1996] and *Nunn et al.* [1997], it is doubtful that spacecraft observations would reveal chorus risers propagating towards the equator at such λ_{S0} points, since this embryonic wave energy would nearly always be masked by counter-propagating waves emitted from the near-equatorial output end of an approximately mirror-image source located across the equator.

[39] Note that as described by *Helliwell* [1967], an additional change in frequency with time can result if the interaction region drifts along the magnetic field line as the interaction proceeds. In the present work, the straight line fit to the (*f*-*t*) spectral form is first attributed to the intrinsic *df*/*dt* for a stationary source, and afterward any residual second-order curvature in the (*f*-*t*) spectral form is attributed to slow drift of the interaction point in the manner described by *Helliwell* [1967], while verifying that any such motion falls within the two bounding limits defined by the particle streaming velocity and the wave group velocity.

3.3. Optimal Source Parameters

[40] The model developed above is applied to a given individual chorus emission to resolve the optimal source parameters as follows. For a discrete chorus emission observed at a given spacecraft location (L_p, λ_p), a small number $3 \leq N \leq 5$ of measured frequency-time-wave normal triples (f, t_p, θ_p) are selected to represent the emission (Figures 4a and 4c) and an initial estimate for the source location along with permissible spatial bounds are determined by tracing three distinct sets of N-ray bundles (one bundle each for θ_p, $\theta_p - \sigma$, and $\theta_p + \sigma$, from Figure 4c) from the observation point back toward, and slightly beyond, the magnetic equator, as discussed in section 3.1. Each (f, t_p, θ_p) triple thus becomes associated with an effective wave emission point in the source region as specified by a corresponding quintuple (f, t_s, L_s, λ_s, θ_s). As a practical expedient, all N source points are considered as sharing a common L_s, while the N source latitudes λ_s and wave normals θ_s along L_s are allowed to take distinct values for each frequency as required during subsequent iteration for best fit to the observed data.

[41] Rays are then traced forward from each of the N source points to the spacecraft to obtain computed estimates of the chorus properties to be compared against the measured (f, t_p, qp) triples. In this regard, when assessing error between simulated and observed triples, it is more convenient to work in terms of estimated frequency for each specific time ($\hat{f}$, t_p, $\hat{\theta}_p$) rather than estimated arrival time for each specific frequency (f, $\hat{t}_p$, $\hat{\theta}_p$), owing both to the form of (2), and the need to avoid singularities for those occasional emissions which at times manifest $df/dt \simeq 0$.

[42] The optimum solution is thus defined by that combination of free source parameters L_s and $(\lambda_s, \theta_s)_i$, $i = 1 \ldots N$, for which the following goals are attained: (1) waves are emitted from a set of source points λ_s distributed along L_s in a way that represents a physically well-behaved emission source, (2) the source wave normal angles θ_s take values consistent with viable electromagnetic whistler-mode refractive index values and reasonable resonant energies for first-order gyroresonant electrons consistent with equation (1), (3) the ray paths arrive at the spacecraft location with negligible spatial error $\hat{L}_p \simeq L_p$ and with estimated wave normals $\hat{\theta}_p$ which fall within one standard deviation of the measured values θ_p, and (4) the reconstructed ($\hat{f}$-t_p) behavior, after accounting for the combined effects of source intrinsic *df*/*dt*, spread in source latitude λ_s, and frequency-time dispersion over the propagation paths, matches the observed (f-t_p) within the spectrogram Δf-Δt resolution uncertainty.

[43] These simultaneous objectives define a moderately difficult constrained multivariate optimization problem since no single parameter may be adjusted without some compensating adjustment being required in another in order to preserve the arrival of all rays paths at the observation point with the correct (*f*-*t*) and wave normals. Accordingly, a simplex method is employed which iteratively adjusts the common L_s and the set of N pairs (λ_s, θ_s), each time retracing the rays from the N wave emission points to the spacecraft to obtain estimated $\hat{L}_p$, $\hat{\theta}_p$ and $\hat{f}_p$, while minimizing the weighted error function

$$\text{err} = \sum_N a|\hat{L}_p - L_p| + b|\hat{\theta}_p - \theta_p|^2 + c|\hat{f}(t_p) - f(t_p)|, \quad (3)$$

where a, b, and c are empirically chosen to promote fast, balanced convergence to the goals listed above. Note that not squaring the L_p and f error terms helps ensure that the rays pass always strictly through the spacecraft point with the correct (*f*-*t*) spectral form, while squaring the θ_p term allows a more generous tolerance on the wave normal fit, consistent with the greater relative uncertainty in measured θ_p than in L_p, f, and t. The error surface turns out to be well-behaved, so that the solution varies smoothly about the eventual optimum values, indicating robustness both to measurement error and to small perturbations in the underlying physical parameters. Conversely, once the optimum solution is identified, no appreciably different set of source parameters is able to reproduce the observed chorus emission with the same fidelity.

4. Chorus Source Characteristics

[44] This section presents detailed source region solutions for cases representing three of the four general types of chorus emissions mentioned herein, namely lower-band risers, lower-band fallers, and upper-band risers (upper-band fallers were not observed on this orbit pass).

4.1. Upper-Band Rising Chorus Emission

[45] Figure 5 shows the solution for the example upper-band riser of Figure 4. In this case the close proximity of the spacecraft to the emission source minimizes opportunity for appreciable error to accumulate over the ray paths which might arise from imperfect knowledge of the cold plasma distribution, thereby building confidence in the solution technique.

[46] Figure 5a shows the solution ray paths (red) emanating from source points (red) below the magnetic equator near $\lambda_s \simeq -3°$ and propagating through and beyond the spacecraft point (open circle). The line segments (black) indicate the local wave normal angles at the source and spacecraft points, respectively. Figure 5b shows both the observed and reconstructed wave normals (black) and ray

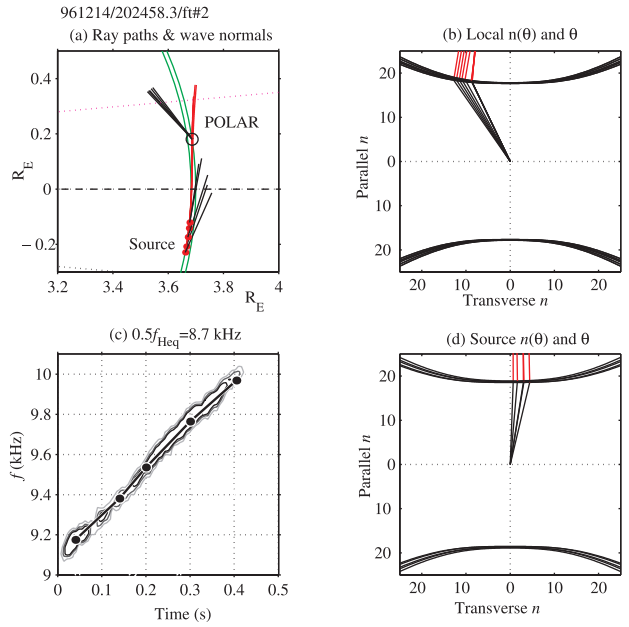

Figure 5. Upper-band chorus riser solution. (a) Ray paths (red lines) from source to spacecraft in relation to POLAR orbit and plasma density model (derived from f_{UHR}). (b) Refractive index (n) surface at spacecraft location with wave normal and ray path in local field-aligned coordinates. (c) Frequency-time match between data and modeled emission (d) Refractive index surface at deduced source location.

directions (red) against the refractive index surface which prevails at the observation point. Figure 5c confirms that the estimated ($\hat{f}$-t) behavior replicates the observed (f-t) behavior. Finally, Figure 5d shows the deduced wave normals (black) and launch ray paths (red) against the refractive index in the source region. Here the wave normals are near zero, albeit slightly positive. In view of the simple shape of the refractive index surface in this frequency range ($f \leq 0.5f_{Heq}$), the corresponding source ray vectors are naturally parallel to the static magnetic field $\mathbf{B_o}$.

[47] Note that the slight positive bias in wave normal values at the source actually provides a slight earthward bias in the ray path launch angle, which promotes natural field-alignment over greater distance as compared with rays for which the initial wave normals and thus launch angles are exactly zero. Whether or not this rather small bias and greater field-aligned distance is significant is uncertain. Meanwhile the wave normals themselves exhibit a rotation from positive (clockwise) values at the source to negative values at the spacecraft, in accord with Snell's Law. This counter-clockwise rotation occurs because this upper-band chorus emission Figure 4 is at a location only slightly beyond the plasmapause in a region where the cold plasma density gradient is large, as can be seen from Figure 2. This gradient controls the ray trajectories as well as the wave normal behavior, causing the wave normals to rotate earthward during the propagation between the source and observation points. In other regions in which cold plasma density gradients are small, the gradients in the static magnetic field instead control the ray trajectories, causing the wave normals to rotate away from the Earth, as evident in the next cases.

4.2. Lower-Band Rising Chorus Emission

[48] Figure 6 shows the solution for a lower-band riser. In this case, the distance from source to observation point is much greater and the source is in a region of relatively small cold plasma density gradient, nonetheless a solution is found which fits the constraints just as well as for the close proximity case.

[49] Figure 6a indicates that the embryonic source point is located at $\lambda_s \simeq -5°$, a value which is not unreasonable in the general context of magnetospheric emissions [c.f., *Dowden,* 1971]. Figure 6d shows that the source emission angle is found to be at $\theta_s \simeq -\theta_G$, where θ_G is the Gendrin angle giving minimum value of the refractive index parallel to the static magnetic field. Note in particular that the ray paths at the source (red line segments in Figure 6d) are naturally parallel to $\mathbf{B_o}$, which is consistent with the concave upward curvature in the refractive index surface at wave normal angles $\pm\,\theta_G$.

[50] This result is by no means contrived or assumed in the solution procedure, but follows directly from Snell's law applied to the measured wave normal angle θ_p at the spacecraft location within the cold plasma density determined from the f_{UHR} line in Figure 2, and the error minimizing iteration of section 3. This same Gendrin source wave normal result is obtained for at least ~80% of all lower-band cases examined thus far, including those from other orbit passes.

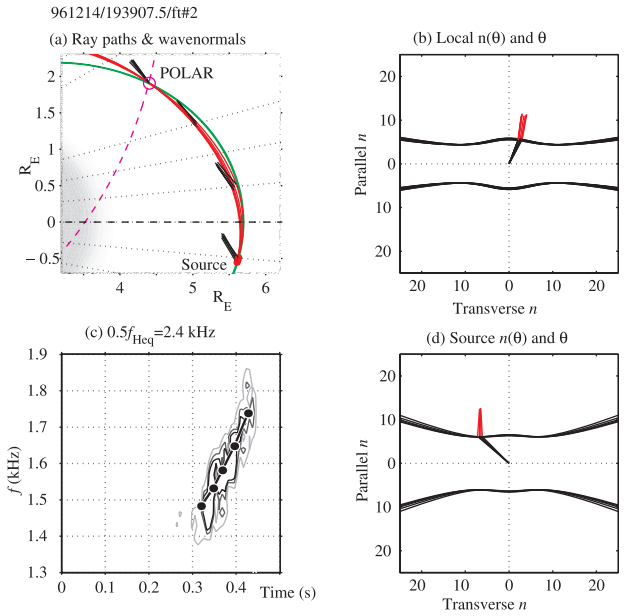

Figure 6. Lower-band chorus riser solution. (a) Ray paths from source to spacecraft in relation to POLAR orbit and plasma density model (derived from f_{UHR}) and trajectory pass. (b) Refractive index (n) surface at spacecraft location with wave normal and ray path in local field-aligned coordinates. (c) Frequency-time match between data and modeled emission. (d) Refractive index surface at deduced source location.

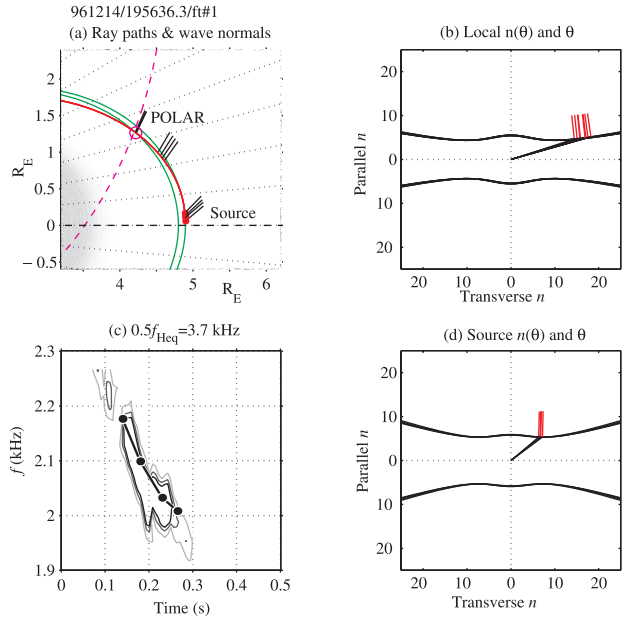

Figure 7. Lower-band faller chorus solution. (a) Ray paths from source to spacecraft in relation to POLAR orbit and plasma density model (derived from f_{UHR}) and trajectory pass. (b) Refractive index (n) surface at spacecraft location with wave normal and ray path in local field-aligned coordinates. (c) Frequency-time match between data and modeled emission. (d) Refractive index surface at deduced source location.

4.3. Lower-Band Falling Chorus Emission

[51] Figure 7 gives the solution for a lower-band faller. Similar to the first case, the source is also in a region of relatively small gradient in the cold plasma density. However, since it is lower-band ($f < 0.5\, f_{Heq}$), the wave normals in the source region are at the Gendrin angle $\theta_s \simeq +\theta_G$ (Figure 7d), and because it is a faller, the source latitude is north of the equator at $\lambda_s \simeq +1°$ (Figure 7a), consistent with northward propagating emissions manifesting $df/dt < 0$ [*Helliwell*, 1967; *Nunn and Smith*, 1996; *Nunn et al.*, 1997]. It is interesting that in this case the measured wave normals are nearly at the resonance cone angle (Figure 7c) at the spacecraft latitude $\lambda_p \simeq 23°$. It is likely that after a few more kilometers of northward propagation, these waves would be quickly extinguished by Landau damping.

4.4. Chorus Ensemble Mosaic

[52] Figure 8 shows ray paths and wave normal angles determined by the model fitting procedure for an ensemble of 10 chorus emissions distributed over this dawn-sector orbit pass in one-for-one association with their respective embryonic source points. Upper-band chorus rays are shown in red, lower-band chorus-rays are shown in blue, and wave normal angles are indicated by the black line segments. Meanwhile, the riser/faller nature of each may be deduced by noting whether the source points are below/above the equatorial plane, respectively.

[53] These cases were chosen based on good signal to noise ratio, good isolation from neighboring chorus emissions and background hiss, and minimal scatter in the measured wave normal values. In all cases the sources are found to have emission wave normals at what may be referred to as the generalized Gendrin angle, namely $\theta_s \simeq \theta_G$ for $f/f_{Heq} \leq 0.5$, and $\theta_s \simeq 0$ for $f/f_{Heq} \geq 0.5$, for which the value of the refractive index parallel to the static magnetic field is minimized. This result holds even as the observed wave normals take on a wide variety of angles at the observation points. In other words, it would appear that the great diversity of wave normal angles observed among an ensemble of discrete chorus emissions can be readily accounted for by the natural evolution in wave normal along the peculiar ray paths from respective sources which universally appear to emit waves at the generalized Gendrin angle. Conversely, the diversity of wave normal angles observed at the various spacecraft locations does not in itself indicate the need for more than one distinct set of emission characteristics for each taxonomic chorus category (i.e., upper/lower-band riser/faller).

[54] A few additional results are evident from Figure 8. The first regards the question of whether lower-band emissions are likely to be gyrotropic (i.e., emitting waves with $\theta_s \simeq \theta_G$ at all azimuthal angles). The answer appear to be yes, as deduced by noting that while the three lower-band risers (blue rays with source points below the equator) in the vicinity of $L \simeq 6$ have source wave normals $\theta_s \simeq -\theta_G$, there is a contrasting example of a lower-band riser close to $L \simeq 4$ which has $\theta_s \simeq +\theta_G$. At the same time, since the waves from the $L \simeq 4$ source arrive at the spacecraft with wave normal angles near the resonance cone (c.f., Figure 7b for the lower-band faller near $L \simeq 5$), they will likely soon be Landau damped at higher latitudes. Extending this expectation to the other lower-band sources near $L \simeq 6$, one can reasonably conclude that any $\theta_s \simeq +\theta_G$ waves emitted by

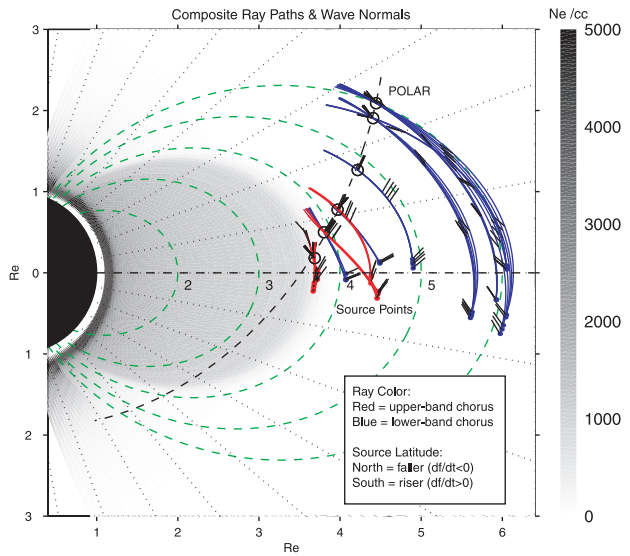

Figure 8. Composite of resulting ray traced source regions for 10 distinct chorus emissions spanning epochs 1943.13 (higher L-shells) to 2024.58 (lower L-shells) on 961214, including a mix of upper-band risers, lower-band risers and lower-band fallers. Chorus fallers have source regions on the same side of the magnetic equator as the observing spacecraft; chorus risers have source regions across the equator. Frequency bands for these sources follow $0.5f_{Heq}$ and $0.35f_{Heq}$ with L-shell as in Figure 1.

these sources are likely to have been strongly damped before reaching the high latitudes sampled by this particular spacecraft trajectory, explaining their absence.

[55] The second regards the effective beam width of a given source. While the following inference is somewhat crude, the two upper-band risers near $L \simeq 4.4$ and $L \simeq 4.5$ (red rays below the magnetic equator) can arguably be taken as representative of a single source (since the rays from the $L \simeq 4.5$ source pass through the $L \simeq 4.4$ source) whose rays spread out to distinct observation points separated by $\Delta L = 0.3$ and $\Delta\lambda = 3.6°$. Whether or not this spread underestimates or overestimates then beam width of a single source can be readily addressed by further ray tracing studies, and ultimately resolved by simultaneous multispacecraft observations.

5. Discussion and Summary

5.1 Discussion

[56] The remarkable feature of the results presented in section 4 is the simple property that the source emission angle for chorus appears to invariably be near that angle for which the ray angle is parallel to $\mathbf{B_o}$ at the wave emission points. Furthermore, for rising emissions, the source is located such that the wave energy from the embryonic source point propagates toward and across the geomagnetic equator. In some cases the embryonic source point appears to be located as much as 5° from the magnetic equator.

[57] The Gendrin angle result can be understood by viewing the chorus emission as a wave packet with finite temporal (and thus spatial) extent, which is amplified during the generation process. The special nonzero Gendrin angle for $f/f_{Heq} \leq 0.5$ keeps the chorus wave packet moving along the same magnetic field line so that the cumulative time for its interaction with electrons is maximized.

[58] According to the present model, the embryonic emission in the source region begins at an intensity near that of background noise levels and is amplified significantly only upon reaching or perhaps crossing the magnetic equator. It is believed that an amplification of up to 40 dB can occur through a gyroresonance interaction with a population of highly anisotropic energetic electrons confined to the vicinity of the magnetic equator because of their very high pitch angles. Note that energetic electron populations of this type have been observed on the POLAR spacecraft in association with VLF emissions within the plasmasphere [*Bell et al.*, 2000].

[59] In light of this amplification process, the present result, which indicates some measure of equatorward propagation (for risers), does not conflict in any way with the recent work of *LeDocq et al.* [1998], who used PWI data from POLAR to show that almost all chorus emissions were observed to be propagating away from the magnetic equator, even when the spacecraft was within a few degrees of this location. This result is actually to be expected since low amplitude embryonic chorus emissions passing the spacecraft on their way to the equator would likely be indistinguishable from background noise and/or would be masked by counter-propagating chorus waves emitted from a conjugate source located across the equator from the point of observation.

[60] To further understand why the generalized Gendrin solution might arise, it is instructive to explore the effects of small deviations about the optimal parameter values for frequencies above and below the minimum and maximum frequency limits of a particular chorus emission. Accordingly, Figure 9 presents ray paths for systematic paired combinations of θ_s and $\Lambda = f/f_{Heq}$. The three lower-most panels show three disjoint sets of wave normals ($-40 \leq \theta_s < -10$, $-10 \leq \theta_s \leq -20$, and $20 \leq \theta < 45$) plotted with respective initial ray path directions against the prevailing refractive index surface at the source point. The 3×3 arrangement of panels above shows corresponding ray paths through a representative interaction region for each wave normal group (left to right) at three values of normalized frequency $\Lambda = f/f_{Heq} = 0.64$, 0.52, and 0.40 (top down), all for the same fixed elapsed group time $t_{gf} = 0.06$ s. The center-3×3 panel shows that rays for the central wave normal group at $f/f_{Heq} = 0.52$ corresponding to the optimal solution determined in section 4 remain the most tightly focused and also the most field aligned over the greatest distance, thus maximizing the wave intensity and wave/particle interaction length for this parameter combination.

[61] This focusing and alignment effect suggests the following sequence of events leading to spontaneous generation of nonducted chorus. First note that the minimal ray path defocusing and maximal field alignment together constitute a type of natural tuned filter promoting greater coherent wave intensity over longer field-aligned paths for $f/f_{Heq} = 0.52$ than for other appreciably different frequencies. Thus whenever some sufficiently anisotropic distribution of counter-streaming particles radiating random wave energy over a generally broad range of frequencies and wave normals passes through this particular region, the natural tuning effect enhances the wave power density along the field line for $f/f_{Heq} = 0.52$ and $\theta \simeq 0 \pm \epsilon$, where ϵ is some small suitable spread in wave normal angle, thereby promoting the conversion of the stochastic noise into coherent waves, notably for wave propagation upstream toward new instreaming particles. Then provided such anisotropic particle distribution persists for some critical duration, the amplitude of $f/f_{Heq} = 0.52$ waves along this field line presumably grow to a level for which incoming upstream particles begin to become significantly phase-bunched within the region of tightly focused rays paths, thus forming a classic helical resonant current structure associated with the backward wave oscillator mechanism [*Helliwell*, 1967; *Trakhtengerts*, 1999]. Since the above scenario has all the ingredients necessary for nonlinear wave/particle feedback, sudden explosive wave growth would likely occur, giving birth to a single discrete chorus emission at this favored frequency.

[62] Subsequently, as the intrinsic df/dt (equation (2)) associated with the wave/particle feedback mechanism takes effect, the wave frequency increases with time ($df/dt > 0$ for this example), thus producing a rising tone chorus emission. The emission frequency would likely continue to increase until it reaches some value of f/f_{Heq} at which the ray paths no longer remain sufficiently focused and/or aligned along the same field line to maintain the intensity required to phase-bunch fresh incoming particles, so that the emission naturally self-terminates. Finally, once all traces of coherent wave energy departs

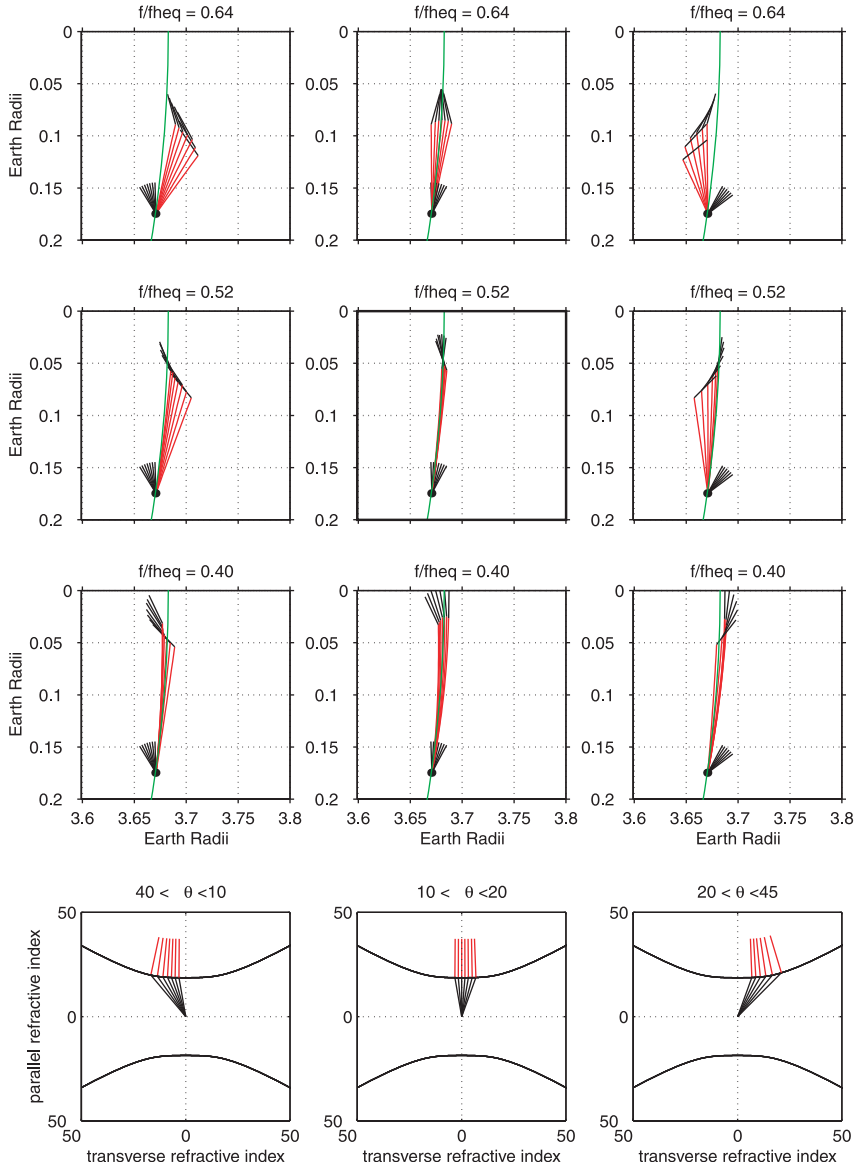

Figure 9. Explorative ray bundles for upper-band chorus. The three lower panels indicate three disjoint groups of wave normals and initial ray path directions on the prevailing refractive index surface at the source point. The panels above show ray paths propagated through a model interaction region for each wave normal group (left to right) and for three values of f/f_{Heq} (top down). The rays for the central wave normal group and f/fh_{eq} = 0.52 remain the most tightly focused and the most field aligned over the greatest distance, offering insight into why chorus occurs for this parameter combination.

the interaction region, the process is free to begin again at the original starting frequency.

[63] Note that although the preceding scenario is more or less a plausibility argument, the underlying factors leading to the natural filtering effect promoting conversion of stochastic wave noise to coherent waves are solidly established. In short, it appears that when nonducted upper-band rising chorus occurs (in this representative example), it starts at the embryonic latitude $|\lambda| \simeq 3^{\circ}$, wave normal angle $\theta \simeq 0 \pm \epsilon$, and starting frequency $f/f_{Heq} \simeq 0.52$ quite simply because in a dipole magnetosphere with typical prevailing cold plasma densities beyond the plasmapause, this combination of parameters leads to ray paths which are maximally focused along a viable source field line, thus forming a natural tuned filter.

[64] A similar situation holds for the lower-band riser as shown in Figure 10. Here the solution from section 4 is identified by the panel labeled $f/f_{Heq} = 0.35$ in the left column, for which waves are emitted with $\theta_s \simeq -\theta_G$ and follow ray paths which arrive at the spacecraft with the correct values for observed wave normals (c.f., Figure 6). The remaining panels show rays traced for the same elapsed time as the solution. Note that in seven of the eight off-solution cases, the waves at significantly different values of f/f_{Heq} (launched at their own respective Gendrin angles) lead to ray paths which do not reach the spacecraft. This is not to say that wave

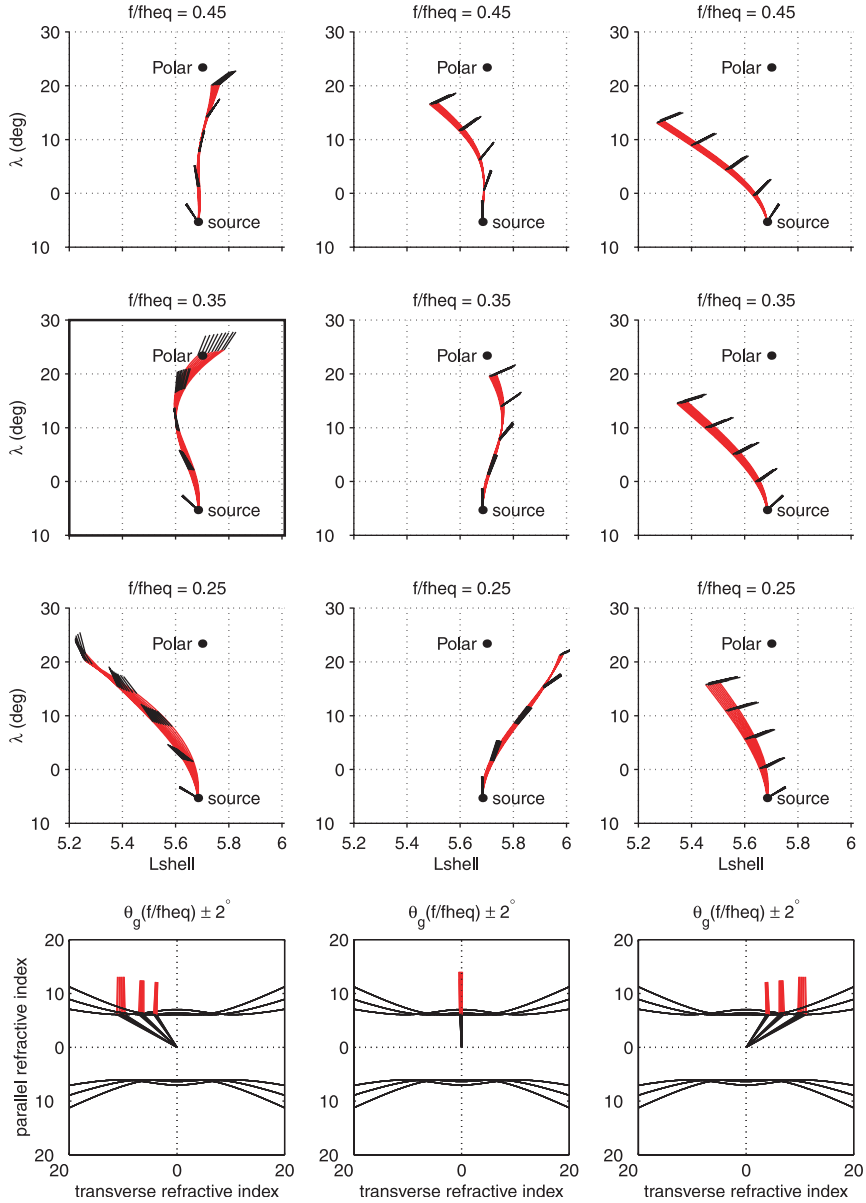

Figure 10. Explorative ray bundles for lower-band chorus. Layout similar to previous figure, but with coordinates L-λ and much longer ray path distances as required to reach the spacecraft. In this case the solution parameters are represented by those for $f/fh_{eq} = 0.35$ shown in the left column, for which the source wave normals are near the Gendrin angle which is located at negative θ values. Rays for the central wave normal group at $f/fh_{eq} = 0.35$ could also reach the observation point, lagging the Gendrin group slightly, but would have wave normals much greater than those actually measured.

emission does not occur for these other frequencies, only that they do not reach the particular spacecraft observation point.

[65] Of special interest is the related case for $f/f_{Heq} = 0.35$ in the center-3 $\times$ 3 panel, which indicates that rays with source wave normals $\theta_s \simeq 0$ could also reach the same observation point, albeit with slight additional time delay with respect to the $\theta_s \simeq 0_G$ group of the same frequency (left column) and with differing received wave normal angle (this scenario is akin to that studied by [*Lefeuvre and Helliwell*, 1985]). It is perhaps not immediately clear why, of the two possible groups, the $\theta_s \simeq -\theta_G$ group is actually observed, while the $\theta_s \simeq 0$ group is not. Some further possible insight is offered by Figure 11, however, which shows 5 ray paths for a small finite wave normal spread $\delta\theta_s = 2^\circ$ about the central value for these two respective wave normal groups to represent equal angular wave power density. Here it is evident that although the rays for the $\theta_s \simeq -\theta_G$ group suffer greater defocusing as they depart the presumed interaction point and thus present lower wave power density to incoming particles than do the $\theta_s \simeq 0$ rays, the Gendrin group nonetheless illuminates the source field line with a coherent wave field over more than 2 times greater distance. Thus on the one hand it may be that the increased latitude coverage for the Gendrin angle waves affords them a critical advantage in the competition to phase-bunch the incoming counter-streaming particles dur-

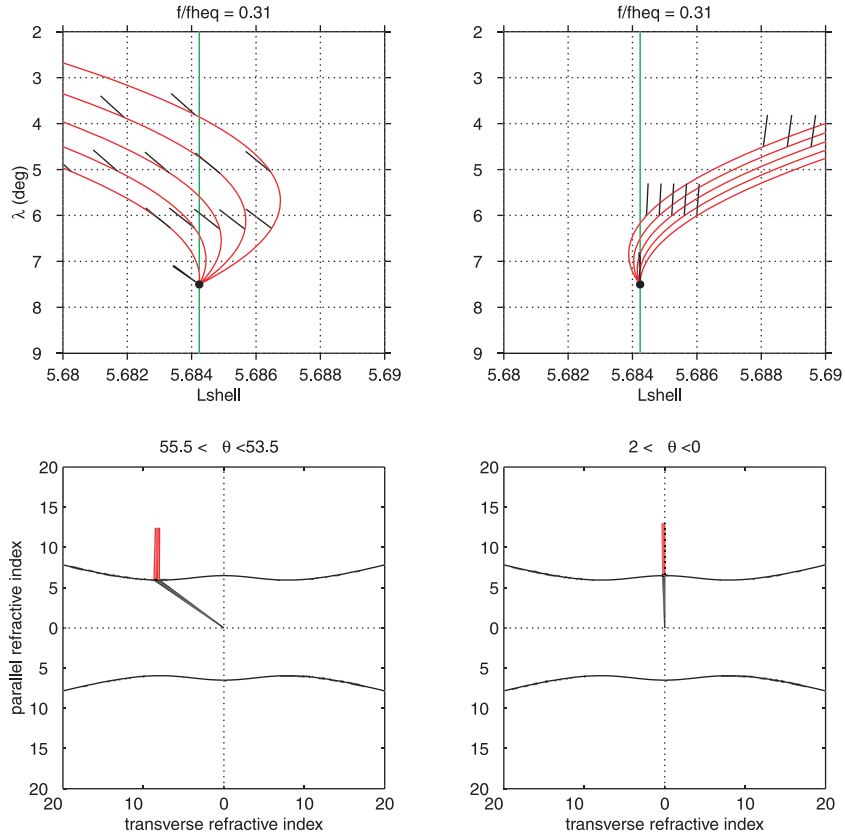

Figure 11. Detailed expanded view of ray bundles at the source region, comparing the Gendrin group ($\theta \simeq \theta_g$) and the central group ($\theta \simeq 0$) at the lower-band riser's leading frequency $f/fh_{eq} = 0.31$. Both groups in principle could have been observed at the spacecraft; however the Gendrin group has more than 2 times greater interaction length for the same $\delta\theta$ spread and hence apparently wins the competition to phase-bunch the incoming particles, leading to the actual mode which is observed at the spacecraft.

ing the embryonic state, possibly even suppressing alternate mode(s), so that the Gendrin angle mode is the only one generated, and therefore the only mode observed. On the other hand, it may be that *both* wave groups are actually generated and emitted together, but that the waves with $\theta_s \simeq 0$ quickly become electrostatic as they propagate (compare the wave normal to ray path angles for each case in the upper panels of Figure 11), and become Landau damped to levels below the background noise before reaching the spacecraft location, so that only the Gendrin group survives to be observed.

5.2. Summary

[66] Six-channel data from the POLAR/PWI instrument has been used to measure the intensity, frequency-time behavior, and wave normal direction of VLF chorus emissions observed in the magnetosphere as the spacecraft moved from $L \simeq 6.5$ to $L \simeq 3.5$ during a dawn-sector orbit pass. The source locations of individual well-defined chorus emissions were determined using a combined emission model and iterative ray tracing technique with the measured wave normal angles and frequency-time characteristics applied as constraints at the spacecraft location in order to deduce characteristics of the emission source.

[67] The results show that with remarkable consistency across different chorus f–t shapes and observation locations (L value and local geomagnetic latitude λ), the emission angle θ_s in the source region takes that frequency-dependent value for which the wave group velocity vector is parallel to the static magnetic field lines. For upper-band chorus ($f \geq 0.5 f_{Heq}$) this angle is indeed $\theta_s \simeq 0$, while for lower-band chorus ($f \leq 0.5\, f_{Heq}$) this angle is $\theta_s \simeq \pm\theta_G$, where θ_G is the so-called Gendrin angle. These respective θ_s values, referred to collectively as the generalized Gendrin angle, lead to wave propagation paths which remain naturally parallel to field lines for typically $\sim 3°-5°$, of latitude, providing ample opportunity for wave/particle interactions with counter-streaming energetic electrons in the absence of any field-aligned cold plasma density enhancements.

[68] In all cases it was found that the chorus source region was near the magnetic equator at slightly off-equatorial latitudes $|\lambda_s| \simeq 3°-5°$, consistent with the region of minimum inhomogeneity in the static magnetic field for the predawn sector. These results apply equally to sources located in regions with large cold plasma density gradients, as well as regions with relatively small cold plasma density gradients. Thus these gradients do not appear to play a strong role in the generation of the chorus emissions.

[69] Finally, a possible physical reason as to why these values should be preferred by the chorus emission process is suggested by further ray tracing studies for small perturbations about the optimum solutions, which show that VLF

whistler mode waves with initial wave normal angles near the generalized Gendrin angle remain more tightly focused and provide coherent illumination over greater distance along a common source field line than do waves at other angles for the two special frequencies $f \simeq 0.35\, f_{Heq}$ and $f \simeq 0.52\, f_{Heq}$, notably in the absence of field aligned cold plasma density irregularities (i.e., ducts). For the preferred solution parameter values, these effects combine to provide more efficient and effective interaction with energetic gyroresonant electrons for equivalent embryonic wave noise power than for off-solution values, thus favoring the resonance, amplification, and emission of chorus waves at the generalized Gendrin angle for either or both of the two preferred emission frequencies.

Appendix 1. The *df*/*dt* for Nunducted Emissions

[70] An outline of the derivation of equation (2) is given below, adapted from *Helliwell* [1967]. The condition for first-order gyroresonance with quasi-longitudinal whistler waves can be written

$$f = f_H \left(\frac{v'_p}{v'_p + v_\parallel} \right)$$

and its variation

$$df = f \left(\frac{df_H}{f_H} + \frac{dv'_p}{v'_p} \right) \frac{f^2}{f_H v'_p} (dv'_p + dv_\parallel),$$

where $v'_p = v_p/\cos\theta$ is the projection of the wave phase velocity along the local static magnetic field line for quasi-longitudinal whistler waves having phase and group velocity

$$v_p = c \frac{f^{1/2}(f_H \cos\theta - f)^{1/2}}{f_N}$$
$$v_g = 2c \frac{f^{1/2}(f_H \cos\theta - f)^{3/2}}{f_N f_H \cos\theta},$$

where f_N is the local plasma frequency and v_g is the group velocity along the wave normal direction. In the present application, the variation in phase velocity becomes

$$dv_p = \frac{c}{2f_N} \left[\frac{(f_H \cos\theta - 2f)df + f \cos\theta\, df_H}{f^{1/2}(f_H \cos\theta - f)^{1/2}} \right]$$

where θ is taken as constant to first order. Upon substitution, the variation in resonant frequency becomes

$$df = \frac{3\Lambda \cos - \Lambda^2(\cos\theta + 2) + \Lambda[\cos\theta - \Lambda(\cos\theta + 1) + \Lambda^2]\tan^2\alpha}{(1+\Lambda)\cos\theta - 2\Lambda^2} df_H,$$

where $\Lambda = f/f_H$ and α is the particle pitch angle. For moderate pitch angles the term involving $\tan^2\alpha$ is negligible and can be ignored. Meanwhile, the time interval *dt* required for an incremental frequency change *df* to accrue at a fixed reference point in the interaction region is given by

$$dt = dS \left(\frac{1}{v_g} + \frac{1}{v_\parallel} \right),$$

which accounts for downstream particle travel time and upstream wave propagation time over an incremental distance *dS*. Finally, the frequency-time slope *df*/*dt* of the emission observed at a stationary point will be

$$\frac{df}{dt} = \left(\frac{v_g v_\parallel}{v_g + v_\parallel} \right) \left[\frac{3\Lambda \cos\theta - \Lambda^2(\cos\theta + 2)}{(1+\Lambda)\cos\theta - 2\Lambda^2} \right] \frac{df_H}{dS},$$

which thus establishes (2). Note that for purely parallel wave propagation, $\cos\theta \rightarrow 1$, so that the term in brackets becomes

$$\left[\frac{3\Lambda(1-\Lambda)}{(1+2\Lambda)(1-\Lambda)} \right] = \left[\frac{3\Lambda}{(1+2\Lambda)} \right],$$

which recovers equation (14) of *Helliwell* [1967] for ducted emissions.

[71] **Acknowledgments.** Janet G. Luhman thanks the referees for their assistance in evaluating this paper.

References

Bell, T. F., The wave magnetic field amplitude threshold for nonlinear trapping of energetic gyroresonant and landau resonant electrons by non-ducted vlf waves in the magnetosphere, *J. Geophys. Res.*, *91*, 4365–4379, 1986.

Bell, T. F., U. S. Inan, R. A. Helliwell, and J. D. Scudder, Simultaneous triggered vlf emissions and energetic electron distributions observed on polar with phi and hydra, *Geophys. Res. Lett.*, *27*, 165–168, 2000.

Brice, N., An explanation of triggered very-low-frequency emissions, *J. Geophys. Res.*, *68*, 4626–4628, 1963.

Burtis, W. J., and R. A. Helliwell, Banded chorus—a new type of vlf radiation observed in the magnetosphere by Ogo 1 and Ogo 3, *J. Geophys. Res.*, *74*, 3002–3010, 1969.

Burtis, W. J., and R. A. Helliwell, Magnetospheric chorus: Amplitude and growth rate, *J. Geophys. Res.*, *80*, 3265–3270, 1975.

Burtis, W. J., and R. A. Helliwell, Magnetospheric chorus: Occurrence patterns and normalized frequency, *Planet Space Sci.*, *25*, 1007–1024, 1976.

Burton, R. K., Critical electron pitch angle anisotropy necessary for chorus generation, *J. Geophys. Res.*, *81*, 4779–4781, 1976.

Burton, R. K., and R. E. Holzer, The origin and propagation of chorus in the outer magnetosphere, *J. Geophys. Res.*, *79*, 1014–1023, 1974.

Cairo, L., and F. Lefeuvre, Localization of sources of ELF/VLF HISS observed in the magnetosphere: Three-dimensional ray tracing, *J. Geophys. Res.*, *91*, 4352–4364, 1986.

Carpenter, D. L., R. R. Anderson, T. F. Bell, and T. R. Miller, A comparison of equatorial electron densities measured by whistlers and by a spacecraft radio technique, *Geophys. Res. Lett.*, *8*, 1107–1110, 1981.

Dowden, R. L., Doppler-shifted cyclotron radiation from electrons: A theory of very low frequency emissions from the exosphere, *J. Geophys. Res.*, *67*, 1745–1750, 1962.

Dowden, R. L., Electron energy spectrum and structure deduced from analysis of VLF discrete emissions by using the Helliwell criterion, *J. Geophys. Res.*, *76*, 3034–3045, 1971.

Dysthe, K. B., Some studies of triggered whistler emissions, *J. Geophys. Res.*, *76*, 6915–6931, 1971.

Gendrin, R., Phase-bunching and other non-linear processes occurring in gyroresonant wave-particle interactions (in magnetosphere), *Astro. Space Sci.*, *28*, 245–266, 1974.

Goldstein, B. E., and B. T. Tsurutani, Wave normal directions of chorus near the equatorial source region, *J. Geophys. Res.*, *89*, 2789–2810, 1984.

Gurnett, D. A., et al., The polar plasma wave instrument, *Space Sci. Rev.*, *71*, 597–622, 1995.

Gurnett, D. A., and B. J. O'Brien, High-latitude geophysical studies with spacecraft Injun 3, 5, Very-low-frequency electromagnetic radiation, *J. Geophys. Res.*, *69*, 65–89, 1964.

Harten, R., and K. Clark, The design features of the GGS wind and polar spacecraft, *Space Sci. Rev.*, *71*, 23–40, 1995.

Hayakawa, M., Y. Yamanaka, M. Parrot, and F. Lefeuvre, The wave normals of magnetospheric chorus emissions observed on board Geos 2, *J. Geophys. Res.*, *89*, 2811–2821, 1984.

Hayakawa, M., K. Hattori, S. Shimakura, M. Parrot, and F. Lefeuvre, Direction finding of chorus emissions in the outer magnetosphere and their generation and propagation, *Planet Space Sci.*, *38*, 135–143, 1990.

Helliwell, R. A., A theory of discrete vlf emissions from the magnetosphere, *J. Geophys. Res.*, *72*, 4773–4790, 1967.

Helliwell, R. A., The role of the Gendrin mode of vlf propagation in the generation of magnetospheric emissions, *Geophys. Res. Lett.*, *22*, 2095–2098, 1995.

Helliwell, R. A., and T. L. Crystal, A feedback model of cyclotron interaction between whistler-mode waves and energetic electrons in the magnetosphere, *J. Geophys. Res.*, *78*, 7357–7371, 1973.

Helliwell, R. A., D. L. Carpenter, and T. R. Miller, Power threshold for growth of coherent vlf signal s in the magnetosphere, *J. Geophys. Res.*, *85*, 3360–3366, 1980.

Inan, U. S., and T. F. Bell, The plasmapause as a vlf wave guide, *J. Geophys. Res.*, *82*, 2819–2827, 1977.

Inan, U. S., Y. T. Chiu, and G. T. Davidson, Whistler-mode chorus and morningside aurorae, *Geophys. Res. Lett.*, *19*, 653–656, 1992.

Isenberg, P. A., H. C. Koons, and J. F. Fennell, Simultaneous observations of energetic electrons and dawnside chorus in geosynchronous orbit, *J. Geophys. Res.*, *87*, 1495–1503, 1982.

Lauben, D. S., U. S. Inan, T. F. Bell, D. L. Kirchner, G. B. Hospodarsky, and J. S. Pickett, Vlf chorus emissions observed by polar during the January 10, 1997, magnetic cloud, *Geophys. Res. Lett.*, *25*, 2995–2998, 1998.

Lauben, D. S., U. S. Inan, and T. F. Bell, Poleward-displaced electron precipitation from lightning-generated oblique whistlers, *Geophys. Res. Lett.*, *26*, 2633–2636, 1999.

LeDocq, M. J., D. A. Gurnett, and G. B. Hospodarsky, Chorus source locations from vlf Poynting flux measurements with the polar spacecraft, *Geophys. Res. Lett.*, *25*, 4063–4066, 1998.

Lefeuvre, F., and R. A. Helliwell, Characterization of the sources of VLF HISS and chorus observed on Geos 1, *J. Geophys. Res.*, *90*, 6419–6438, 1985.

Means, J. D., Use of the three-dimensional covariance matrix in analyzing the polarization properties of plane waves, *J. Geophys. Res.*, *77*, 5551–5559, 1972.

Molvig, K., G. Hilfer, R. H. Miller, and J. Myczkowski, Self-consistent theory of triggered whistler emissions, *J. Geophys. Res.*, *93*, 5665–5683, 1988.

Muto, H., M. Hayakawa, M. Parrot, and F. Lefeuvre, Direction finding of half-gyrofrequency vlf emissions in the off-equatorial region of the magnetosphere and their generation and propagation, *J. Geophys. Res.*, *92*, 7538–7550, 1987.

Nunn, D., A theory of vlf emissions, *Planet Space Sci.*, *19*, 1141–1167, 1971.

Nunn, D., A self-consistent theory of triggered vlf emissions, *Plan. Space Sci.*, *22*, 349–378, 1974.

Nunn, D., The numerical simulation of vlf nonlinear wave-particle interactions in collision-free plasmas using the Vlasov hybrid simulation technique, *Comp. Phys. Comm.*, *60*, 1–25, 1990.

Nunn, D., and A. J. Smith, Numerical simulation of whistler-triggered vlf emissions observed in Antarctica, *J. Geophys. Res.*, *101*, 5261–5277, 1996.

Nunn, D., Y. Omura, H. Matsumoto, I. Nagano, and S. Yagitani, The numerical simulation of vlf chorus and discrete emissions observed on the GEOTAIL spacecraft using a Vlasov code, *J. Geophys. Res.*, *102*, 27,083–27,097, 1997.

Omura, Y., and H. Matsumoto, Computer simulations of basic processes of coherent whistler wave-particle interactions in the magnetosphere, *J. Geophys. Res.*, *87*, 4435–4444, 1982.

Omura, Y., D. Nunn, H. Matsumoto, and M. J. Rycroft, A review of observational, theoretical and numerical studies of vlf triggered emissions, *J. Atmos. Terr. Phys.*, *53*, 351–358, 1991.

Salvati, M. A., U. S. Inan, T. J. Rosenberg, and A. T. Weatherwax, Solar wind control of polar chorus, *Geophys. Res. Lett.*, *27*, 649–652, 2000.

Sazhin, S. S., and M. Hayakawa, Magnetospheric chorus emissions: A review, *Plan. Space Sci.*, *40*, 681–697, 1992.

Skoug, R. M., S. Datta, M. P. McCarthy, and G. K. Parks, A cyclotron resonance model of vlf chorus emissions detected during electron microburst precipitation, *J. Geophys. Res.*, *101*, 21,481–21,491, 1996.

Smith, A. J., and D. Nunn, Numerical simulation of vlf risers, fallers, and hooks observed in Antarctica, *J. Geophys. Res.*, *103*, 6771–6784, 1998.

Stix, T. H., The Theory of Plasma Waves, McGraw-Hill, New York, 1962.

Trakhtengerts, V. Y., Magnetosphere cyclotron maser: Backward wave oscillator generation regime, *J. Geophys. Res.*, *100*, 17,205–17,210, 1995.

Trakhtengerts, V. Y., A generation mechanism for chorus emission, *Ann. Geophys.*, *17*, 95–100, 1999.

Tsurutani, B. T., and E. J. Smith, Postmidnight chorus: a substorm phenomenon, *J. Geophys. Res.*, *79*, 118–127, 1974.

Tsurutani, B. T., and E. J. Smith, Two types of magnetospheric elf chorus and their substorm dependences, *J. Geophys. Res.*, *82*, 5112–5128, 1977.

Vomvoridis, J. L., T. L. Crystal, and J. Denavit, Theory and computer simulations of magnetospheric very low frequency emissions, *J. Geophys. Res.*, *87*, 1473–1489, 1982.

D. S. Lauben, U. S. Inan, and T. F. Bell, STARLab, Stanford University, Stanford, CA 94305-9515, USA. (dsl@leland.stanford.edu)

D. A. Gurnett, Dept. Physics & Astronomy, University of Iowa, Iowa City, IA, 52242, USA.